Japanese Journal of Radiology (2019) 37:165–177
https://doi.org/10.1007/s11604-018-0789-1

ORIGINAL ARTICLE

Imaging of renal cell carcinoma in patients with acquired cystic disease of the kidney: comparison ^{11}C-choline and FDG PET/CT with dynamic contrast-enhanced CT

Kazuhiro Kitajima[1] · Shingo Yamamoto[2] · Yusuke Kawanaka[3] · Takayuki Katsuura[1] · Masahiro Fujita[1] · Yukako Nakanishi[2] · Yusuke Yamada[2] · Takahiko Hashimoto[2] · Toru Suzuki[2] · Shuken Go[2] · Akihiro Kanematsu[2] · Michio Nojima[2] · Koichiro Yamakado[3]

Received: 11 August 2018 / Accepted: 25 October 2018 / Published online: 30 October 2018
© Japan Radiological Society 2018

Abstract

Purpose To evaluate renal cell carcinoma (RCC) findings in acquired cystic disease of the kidney (ACDK) shown by ^{11}C-choline and FDG PET/CT, and contrast-enhanced CT.

Materials and methods Six ACDK patients with 7 RCCs underwent ^{11}C-choline and FDG PET/CT, and contrast-enhanced CT before nephrectomy. Findings obtained with 3 imagings were evaluated and sensitivity detecting RCC was compared using 3-point grading scale (negative, equivocal, positive). The equivocal scale used for SUVmax ranged from 2.0 to 3.0 for PET/CT and a peak enhancement value ranging from 20 to 30 HU was used for CT.

Result The histopathologic subtypes of 7 RCCs were clear-cell ($n=4$) and ACD-associated RCC ($n=3$). The negative/equivocal/positive grading results were 0/0/7 for ^{11}C-choline-PET/CT, 0/3/4 for FDG-PET/CT, and 2/2/3 for CT. Three equivocal cases by FDG-PET/CT were 2 clear-cell RCCs and 1 ACD-associated RCC. CT of 3 ACD-associated RCCs showed negativity for 2 and equivocality for 1. Sensitivity defining equivocal interpretation as negative for ^{11}C-choline-PET/CT, FDG-PET/CT, and CT was 100% (7/7), 57.1% (4/7), and 42.9% (3/7).

Conclusion ^{11}C-choline-PET/CT was more sensitive to detect RCC in ACDK as compared to FDG-PET/CT and contrast-enhanced CT in our series. FDG-PET/CT may be limited for detecting clear-cell RCC, while CT may have difficulty with detection of ACD-associated RCC.

Keywords Renal cell carcinoma (RCC) · Acquired cystic disease of the kidney (ACDK) · Choline · Fluorodeoxyglucose (FDG) · Positron emission tomography/computed tomography (PET/CT)

Introduction

Acquired cystic disease of the kidney (ACDK) is defined as the presence of more than three cysts in either or both kidneys, or an area of the renal parenchyma occupied by such cysts greater than 25% in patients with end-stage renal disease [1, 2]. The most important predisposing factor for ACDK is prolonged duration of dialysis, with the disease occurring in 40–60% of patients with a dialysis duration of 3–5 years and more than 90% in those with a duration of 5–10 years or more [2, 3]. A major clinical concern is that patients with ACDK show an increased prevalence for occurrence of renal cell carcinoma (RCC) [1–3]. It has also been reported that 3–7% of patients with ACDK develop RCCs in their native kidneys and have a 100-times greater risk for such development as compared with the general population [3]. Nearly, all histologic variants of RCC can develop in the background of ACDK, though in recent years 2 new subtypes, acquired cystic disease-associated RCC (ACD-associated RCC) and clear cell-papillary RCC, have been added [4]. Early intervention may prolong the cancer-free survival of affected individuals [2, 5, 6]; thus, periodic imaging examinations are important to detect RCC in an early stage.

Several imaging modalities, including ultrasonography (US) [7], contrast-enhanced computed tomography (CT) [8–10], and magnetic resonance imaging (MRI) [11, 12],

✉ Kazuhiro Kitajima
kitajima@med.kobe-u.ac.jp; kazu10041976@yahoo.co.jp

Extended author information available on the last page of the article

are used for diagnosis of RCC in patients with ACDK. As for screening of patients with ACDK for RCC, dynamic contrast-enhanced CT is the most widely used modality, because it can detect and also allow for differentiation of RCCs from hemorrhagic cysts, which do not show enhancement. However, a false-negative diagnosis of RCC in these patients based on dynamic contrast-enhanced CT results is often seen in clinical practice for several reasons. First, frequently subtypes, such as ACD-associated and papillary RCC, show poor contrast enhancement on dynamic contrast-enhanced CT [9, 13]. Another problem occurs when the observer does not attempt to carefully evaluate contrast enhancement in each mass when there are multiple or numerous acquired cysts. Additionally, even a large carcinoma may sometimes be difficult to diagnose based on contrast-enhanced CT findings in patients with an ACDK when surrounding hemorrhagic cysts make the background inhomogeneous and thus provide camouflage for the neoplasm [9]. Therefore, a more sensitive and accurate imaging tool is anticipated.

Although neither positron emission tomography (PET) with ^{18}F-fluorodeoxyglucose (FDG) or ^{11}C-choline is considered useful to detect renal lesions, due to physiological uptake in the kidneys of patients with normal renal function, those may be useful to diagnose renal lesions in patients with renal failure because of lack of such physiological uptake. To the best of our knowledge, only one group has presented a case report in which FDG-PET was shown useful to detect ACD-associated RCC [13], while there are no known reports demonstrating the diagnostic performance of ^{11}C-choline PET for RCC in ACDK patients. The purpose of the present study was to conduct evaluations of ^{11}C-choline and FDG PET and compare the findings with those of contrast-enhanced CT for detection of RCC in ACDK patients.

Materials and methods

Patients

This prospective study was approved by the ethics committee of our institution (no. 2213). Informed consent was obtained from each patient after the procedure details were fully explained. From August 2016 to April 2017, 6 male patients (age range 29–79 years, median age 66 years) with a suspected of RCC with ACDK on the basis of US, CT, and MRI underwent preoperative ^{11}C-choline and FDG positron emission tomography/computed tomography (PET/CT) and contrast-enhanced CT examinations prior to undergoing a nephrectomy for RCC diagnosed from histological results (Table 1). There have been no patients who were duplicated with 28 patients in our published paper [14]. Clinical diagnosis and treatment option were decided based on information derived from these examinations and previous

Table 1 Patients and tumor imaging characteristics

Patients	Age	Sex	Histological subtype	Duration of dialysis (year)	Long diameter (cm)	SUVmax on FDG-PET	SUVmax on choline-PET	Dynamic contrast-enhanced CT			
								TApre (HU)	TAcor (HU)	TAneph (HU)	PTEV
1	66	M	ACD-associated RCC	16.2	4.3	3.39	5.08	27	34	48	21
(Figure 1)			ACD-associated RCC		3.9	8.72	18.8	52	55	49	3
2	48	M	ACD-associated RCC	11.9	2.6	2.86	3.73	16	20	32	16
(Figure 2)											
3	66	M	Clear cell RCC	6.2	3.2	2.28	6.56	35	102	83	67
4	66	M	Clear cell RCC	6.1	9.4	9.34	5.87	37	54	57	20
5	79	M	Clear cell RCC	3.3	3.2	5.08	9.97	26	91	80	65
6	29	M	Clear cell RCC	5.5	2.5	2.15	3.13	29	81	66	52

several imagings at the Urological Tumor Board Conference with urologists, radiologists, and radiation oncologists. The median duration of dialysis before the operation was 6.2 years (range 3.3–16.2 years). The 3 imaging examinations (^{11}C-choline PET/CT, FDG-PET/CT, contrast-enhanced CT) were conducted within a period of 14 days in each patient and the median time between completion of the final imaging examination and surgery was 18.3 days (12–33 days).

^{11}C-choline PET/CT

^{11}C-choline was synthesized using a commercial module, as described by Hara [15], and used with a CYPRIS-325R cyclotron [Sumitomo Heavy Industries (SHI), Tokyo]. Acquisition of emission scans from the mid-thigh to head was started approximately 6 min after intravenous injection of ^{11}C-choline at 3.0 MBq/kg body weight. All PET/CT examinations were performed using a PET/CT scanner equipped with a 64-multi-detector computed tomography device (Gemini TF64; Philips Medical Systems, Eindhoven, The Netherlands). Whole-body PET acquisition in 3D mode was performed from the mid-thigh to top of the head (1.5 min per bed position, 6–8 bed positions) and reconstructed using the ordered-subset expectation maximization (OSEM) reconstruction algorithm (33 subsets, 3 iterations, 4 mm per slice), with attenuation correction based on low-dose CT (120 kVp, 100 mA, slice thickness 2 mm, transverse field of view 600 mm), which was also used for anatomical correlation.

FDG PET/CT

FDG was synthesized using the nucleophilic substitution method with an FDG-synthesizing instrument F-200 (SHI) and CYPRIS-325R cyclotron (SHI). Patients were instructed to fast for 5 h prior to scanning and blood glucose was measured immediately before injection of FDG at 3.0 MBq/kg body weight. None of the patients had a blood glucose level > 160 mg/dl. Whole-body FDG-PET/CT was performed 60 min after injection of FDG from the top of the head to mid-thigh level, with the same acquisition and reconstruction parameters noted above for ^{11}C-choline PET/CT. No indwelling catheter or diuretic was used.

Dynamic contrast-enhanced CT

Preoperative dynamic contrast-enhanced CT was performed with a 128-multidetector row CT scanner (SOMATOM Definition AS+ , Siemens AG, Erlangen, Germany) at 120 kV and an effective mAs of 220 (CAREDose4D), a beam pitch of 0.6, a collimation of 1.2 × 32 mm, and B31+ medium smooth + image reconstruction. First, pre-contrast CT images were scanned. Next, a total of 100 ml of a nonionic iodinated contrast agent (IopamironInj, Syringe, Bayer Schering Pharma, Berlin, Germany) containing 300 mg of iodine/ml at a dose of 600 mg iodine/kg body weight was intravenously administered using a power injector at a rate of 3.0 ml/s. The time delay for scanning for the corticomedullary phase was 30 s and that for nephrographic phase images was 90 s.

Image analysis

Two experienced readers (Y.K and K.K) with 5 and 10 years of experience with PET/CT, respectively, who had no knowledge of the other imaging results or pathological results, retrospectively interpreted the ^{11}C-choline and FDG PET/CT images, with decisions based on consensus. Semiquantitative analysis of abnormal radiotracer uptake for each primary tumor was also retrospectively performed using the maximum standardized uptake value (SUVmax), calculated as follows: SUV = volume of interest (VOI) radioactivity concentration (Bq/ml)/[injected dose (Bq)/patient weight (g)]. SUVmax, defined as the highest SUV value for pixels with the highest count within the VOI, was determined for the focal areas of uptake and recorded.

Referring to ^{11}C-choline and FDG PET/CT images, the same 2 experienced radiologists (Y.K and K.K) with 7 and 17 years of experience with abdominal CT, respectively, who had no knowledge of the pathological results, retrospectively interpreted all CT images with decisions based on consensus. After the entire slices showing each tumor were

observed, the attenuation values of 3 separate regions of interest (ROIs), which included the solid component of the tumor but excluded blood vessels, calcification, and gross necrosis, were measured within the lesion. In CT images, the solid component shows obvious enhancement after injection of contrast medium and each ROI should be as large as possible to reduce intraobserver variation. The 3 ROIs were placed in corresponding locations on images obtained in the 3 phases. The average attenuation value of the 3 ROIs was calculated to determine the tumor attenuation value in each phase. Pre-contrast phase tumor attenuation (TApre), corticomedullary phase tumor attenuation (TAcor), and nephrographic phase tumor attenuation (TAneph) were used as tumor attenuation values for the pre-contrast, corticomedullary, and nephrographic phases, respectively. The peak enhancement value of the tumor (PTEV) was calculated as the difference between the attenuation value in an enhanced phase (corticomedullary or nephrographic phase) and that in an unenhanced phase. The maximal diameter of each lesion was also measured.

Statistical analysis

The sensitivity of each imaging modality (^{11}C-choline and FDG PET/CT, dynamic contrast-enhanced CT) to detect RCC was scored using a 3-point grading scale (negative, equivocal, positive). The definition of equivocal scale for the tumor was an SUVmax range of 2.0–3.0 in ^{11}C-choline and FDG PET/CT results, and peak enhancement value in a range of 20–30 Hounsfield units (HU) [9, 16] on dynamic contrast-enhanced CT. Sensitivity was calculated by defining equivocal interpretations as negative.

Results

In the 6 examined ACDK patients, 7 RCCs were confirmed by histopathology results (Table 1). One patient had 2 RCCs (1 in each kidney) and 5 had 1 RCC each in a single kidney. The median diameter of the 7 RCCs was 3.2 cm (2.5–9.4 cm). The histopathologic subtypes of the RCCs were clear cell RCC in 4 and ACD-associated RCC in 3 cases.

The mean SUVmax of the tumors in ^{11}C-choline and FDG PET/CT findings was 7.59 ± 5.42 (3.13–18.8) and 4.83 ± 3.03 (2.15–9.34), respectively, with the former modality showing a tendency to be higher, though the difference was not significant ($p = 0.26$, paired t test).

The mean TApre, TAcor, and TAneph values were 31.7 ± 11.2 HU (16–52 HU), 62.4 ± 30.1 HU (20–102 HU), and 59.3 ± 18.3 HU (32–83 HU), respectively. Peak enhancement was observed in the corticomedullary phase in 4 cases (3 clear cell RCCs, 1 ACD-associated RCC) and in the nephrographic phase in 3 cases (2 ACD-associated RCCs, 1 clear cell RCC). The mean PTEV value was 34.9 ± 25.9 HU (3–67 HU). Two representative cases are presented in Figs. 1 and 2.

The grading results for negative/equivocal/positive were 0/0/7 for ^{11}C-choline PET/CT, 0/3/4 for FDG-PET/CT, and 2/2/3 for dynamic contrast-enhanced CT, respectively. The 3 equivocal cases shown by FDG-PET/CT were 2 clear cell RCCs and 1 ACD-associated RCC. Of the 3 ACD-associated RCCs shown by dynamic contrast-enhanced CT, 2 showed negativity and 1 equivocality. Sensitivity for defining the equivocal interpretation as negative was 100% (7/7) for ^{11}C-choline PET/CT, 57.1% (4/7) for FDG-PET/CT, and 42.9% (3/7) for contrast-enhanced CT.

Discussion

For diagnosis of RCC in patients with ACDK, several different imaging modalities are utilized clinically, including US [7], contrast-enhanced CT [8–10], and MRI [11, 12], though each has advantages as well as disadvantages. Although most studies that evaluated the prevalence of RCC in patients with ACDK were based on US findings, the detection rate of RCC by that modality is less than satisfactory. Gulanikar et al. [7] reported that the sensitivity of a screening US examination for diagnosis of RCC in patients with end-stage renal disease (including those with ACDK) was only 36.3%.

Consequently, it is generally agreed that dynamic contrast-enhanced CT is the best imaging technique for diagnosis of RCC in end-stage renal disease patients [8–10]. Although Takebayashi et al. [9] demonstrated that the early enhanced phase of dynamic contrast-enhanced CT was able

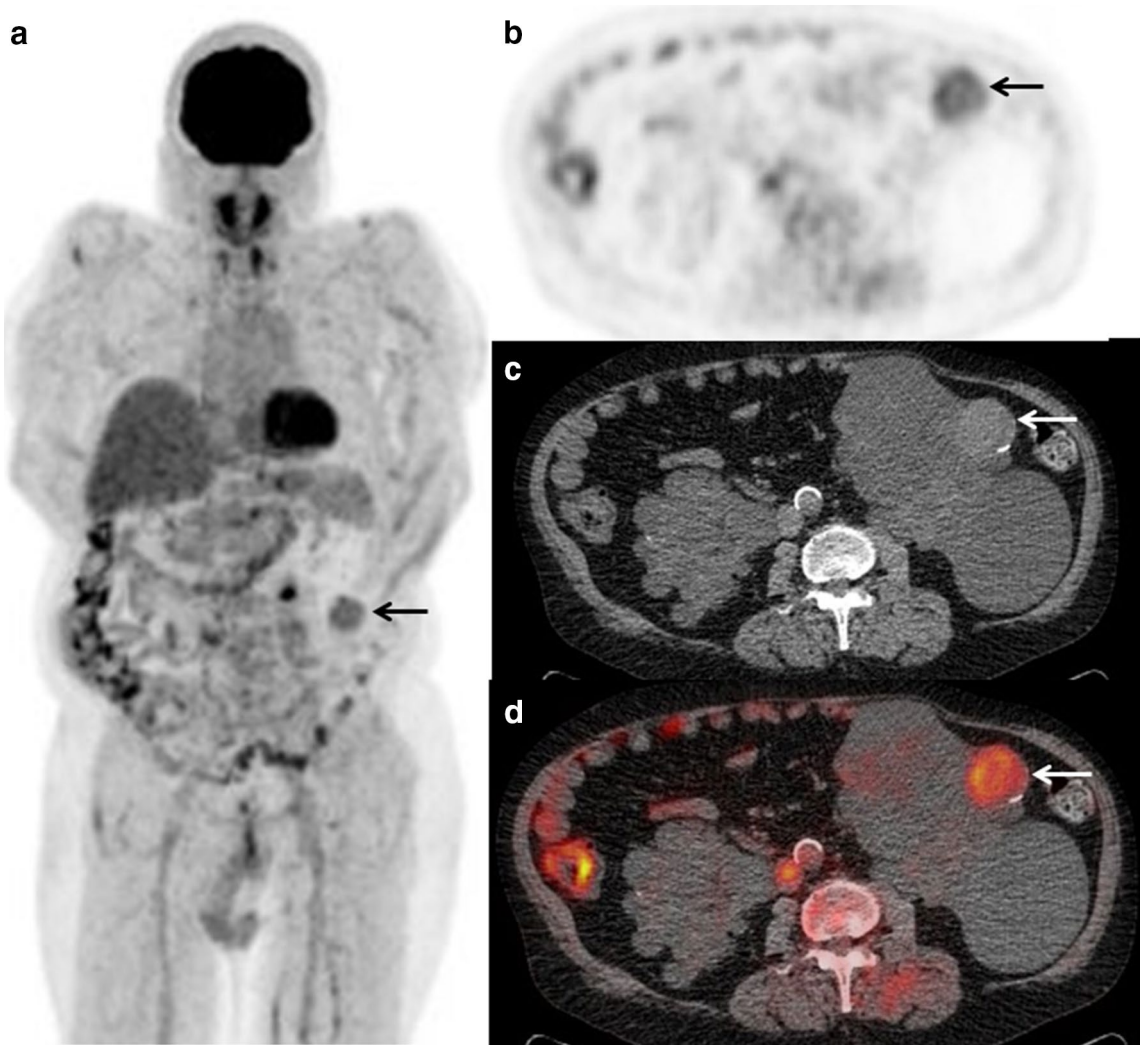

Fig. 1 Images of 2 acquired cystic disease-associated renal cell carcinomas (ACD-associated RCCs), both in left kidney, in a 66-year-old male with acquired cystic disease of the kidney. Maximum intensity projection (MIP) obtained with **a** ^{18}F-fluorodeoxyglucose-positron emission tomography (FDG-PET), **b** axial FDG-PET, **c** axial computed tomography (CT), and **d** fused FDG-PET/CT showing mild FDG uptake [maximum standardized uptake value (SUVmax) 3.39] in left renal hyperdense mass (arrows). MIP obtained with **e** ^{11}C-choline PET, **f** axial ^{11}C-choline PET, **g** axial CT, and **h** fused ^{11}C-choline PET/CT showing moderate ^{11}C-choline uptake (SUVmax 5.08) in left renal hyperdense mass (arrows) corresponding to the same lesion shown in **a**–**d**. **i**–**k** Dynamic contrast-enhance CT image showing a 4.3-cm sized left renal mass with delayed mild enhancement (arrows) corresponding to the same lesion shown in **a**–**h**. The tumor attenuation values in the **i** pre-contrast, **j** corticomedullary, and **k** nephrographic phases were 27, 34, and 48 HU, respectively. MIP obtained with **l** FDG-PET, **m** axial FDG-PET, **n** axial CT, and **o** fused FDG-PET/CT showing high FDG uptake (SUVmax 8.72) in the other left renal hyperdense mass (arrows). MIP obtained with **p** ^{11}C-choline PET, **q** axial ^{11}C-choline PET, **r** axial CT, and **s** fused ^{11}C-choline PET/CT showing very strong ^{11}C-choline uptake (SUVmax 18.8) in left renal hyperdense mass (arrows) corresponding to the same lesion shown in **l**–**o**. **t**–**v** Dynamic contrast-enhanced CT showing a 3.9-cm sized left renal mass with almost no enhancement (arrows) corresponding to the same lesion shown in **l**–**s**. The tumor attenuation values in the **t** pre-contrast, **u** corticomedullary, and **v** nephrographic phases were 52, 55, and 49 HU, respectively

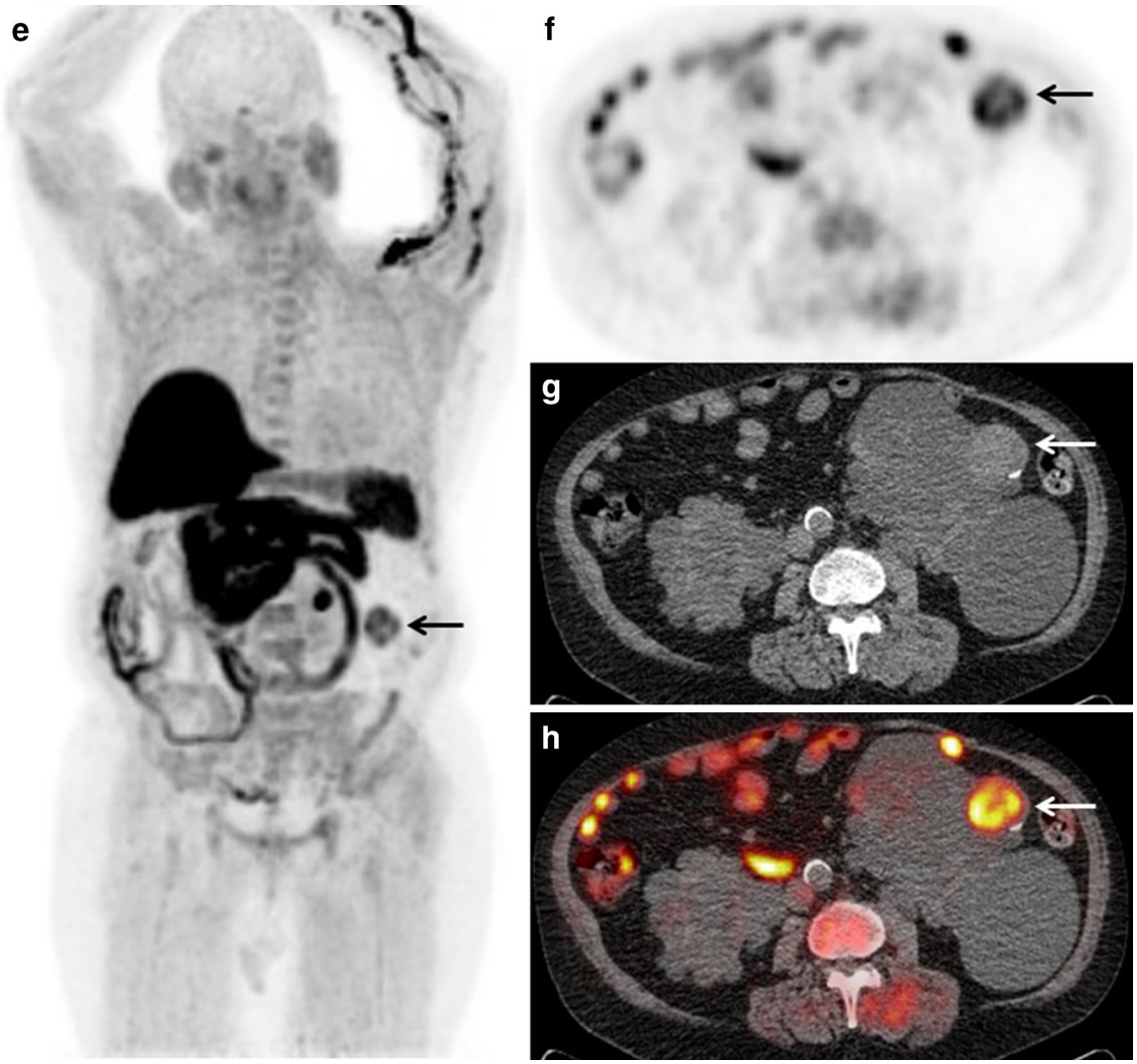

Fig. 1 (continued)

to detect all RCCs in 18 ACDK patients (sensitivity 100%), the histological subtype was not clarified. That modality may easily detect clear cell RCC in ACDK patients because that type of tumor is mostly hypervascular. On the other hand, RCC subtypes frequently seen in patients with ACDK, such as ACD-associated RCC and papillary RCC, have poor contrast enhancement in dynamic contrast-enhanced CT imaging and diagnosis of these types of RCC is difficult with use of that modality [13]. The same as in Ishikawa's report [13], in our series, all 3 (100%) cases of ACD-associated RCC had a false-negative finding in dynamic contrast-enhanced CT, whereas only 1 (25%) case of clear cell RCC was false negative.

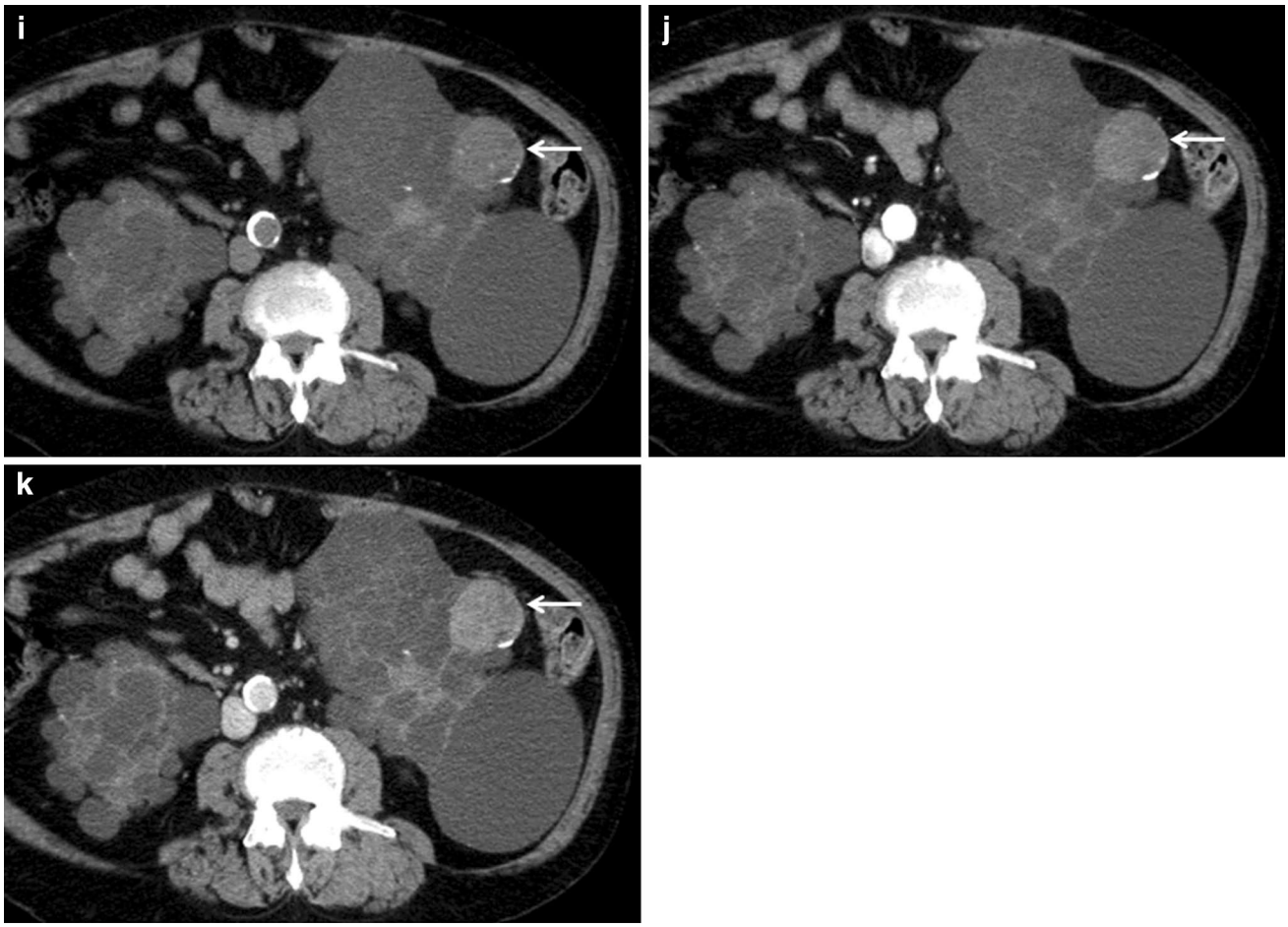

Fig. 1 (continued)

Although gadolinium-enhanced MRI can also allow for differentiation of RCCs from hemorrhagic cysts [11], it is now contraindicated for dialysis patients because of recently reported concerns regarding induction of nephrogenic systemic fibrosis by the contrast agent [17]. Akita et al. [12] demonstrated the utility of diffusion-weighed imaging (DWI) without use of contrast material for diagnosis of RCC in 7 patients with ACDK.

Ishikawa et al. [13] reported an 8.5-cm sized ACD-associated RCC that showed an SUVmax of 3.8 in FDG-PET/CT findings. In the present series, FDG-PET/CT revealed 3 ACD-associated RCCs with SUVmax values of 2.86, 3.39, and 8.72, respectively. Most ACD-associated RCCs are FDG-avid tumors, whereas a clear cell RCC in patients with normal renal function sometimes presents a low SUVmax value [18]. In our 4 patients with renal failure, FDG-PET findings showed negative uptake in 2 (50%) and equivocal

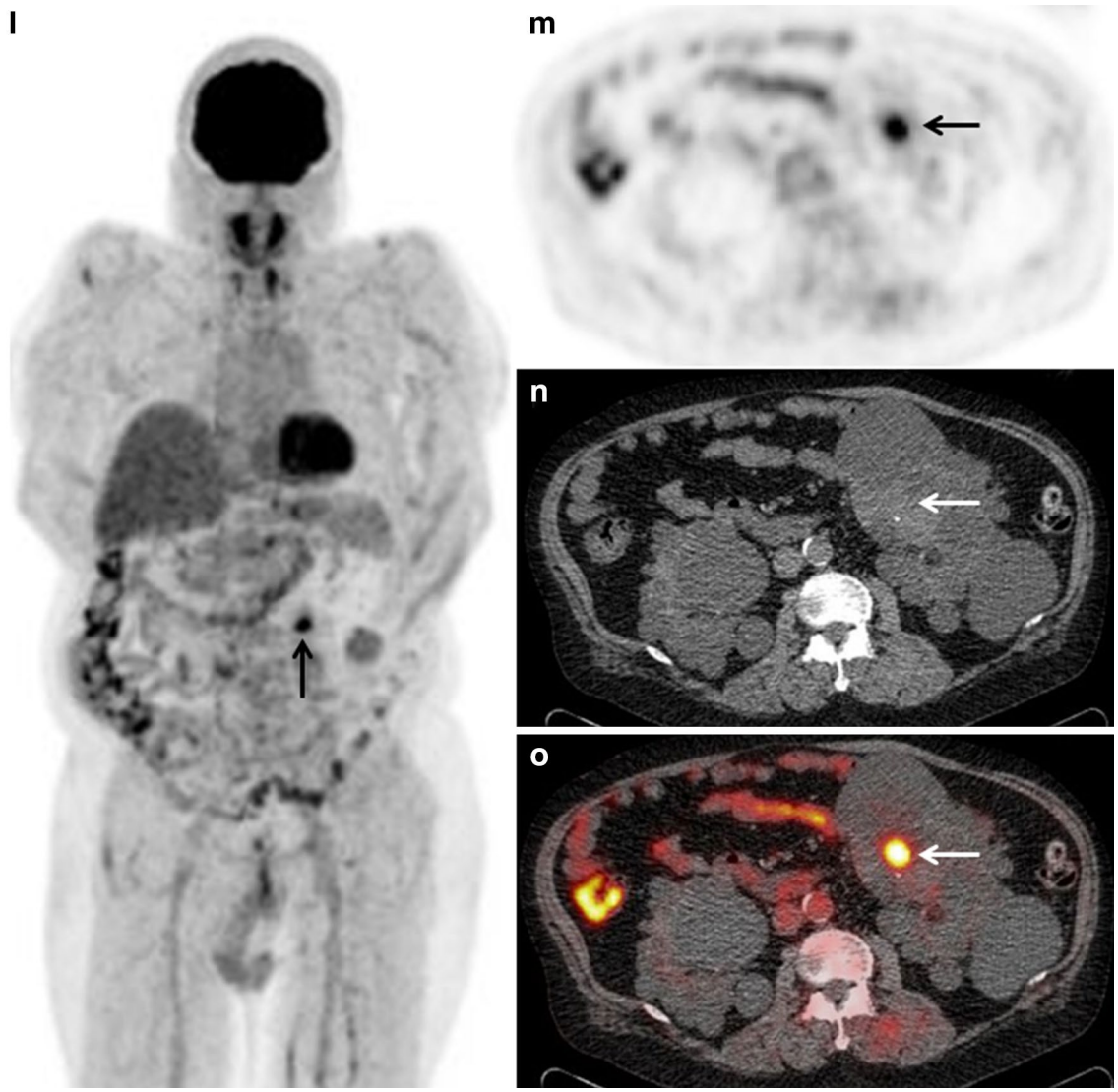

Fig. 1 (continued)

uptake in 2 (50%). On the other hand, ^{11}C-choline PET showed positive uptake in all patients (100%) in our series regardless of the presence of an ACD-associated or clear cell RCC. Although the usefulness of ^{11}C-choline PET for detection of an RCC in ACDK patients must be confirmed with a larger cohort, 2 other case reports [19, 20] and one original research paper [14] have noted its usefulness for detecting RCC lesions in patients with normal renal function.

This study had several limitations. First, this is a retrospective review of a small number of patients.

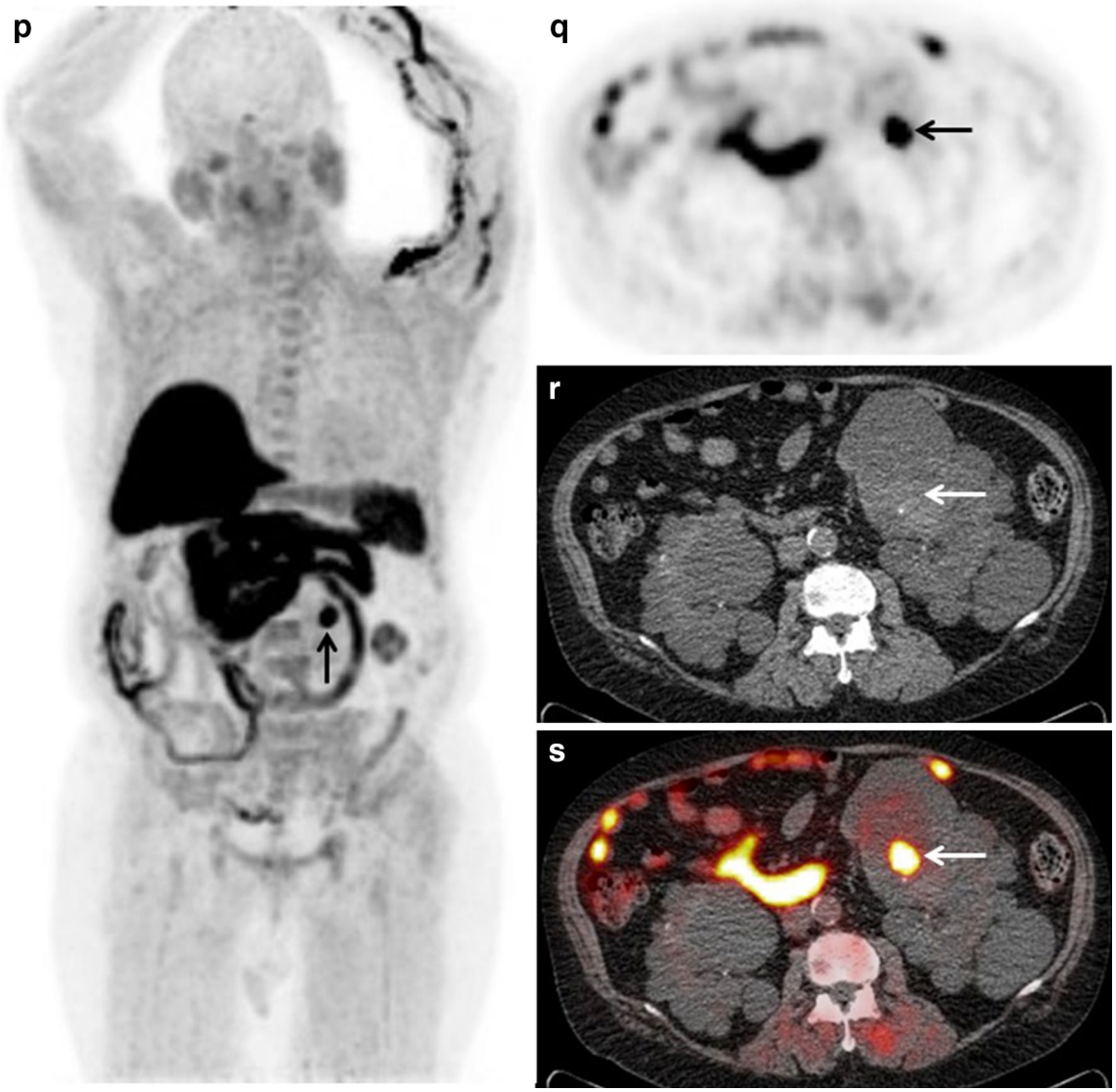

Fig. 1 (continued)

Nevertheless, we believe that our findings can serve as a first step toward a further prospective study with a greater number of patients. Second, our cohort included only ACDK patients with an RCC, thus the specificity of the imaging modalities examined could not be evaluated. Finally, MRI was performed in only 2 of the 6 patients and those results were not evaluated.

In conclusion, ^{11}C-choline PET/CT was shown to be more sensitive to detect RCC in patients with ACDK as compared to FDG-PET/CT and dynamic

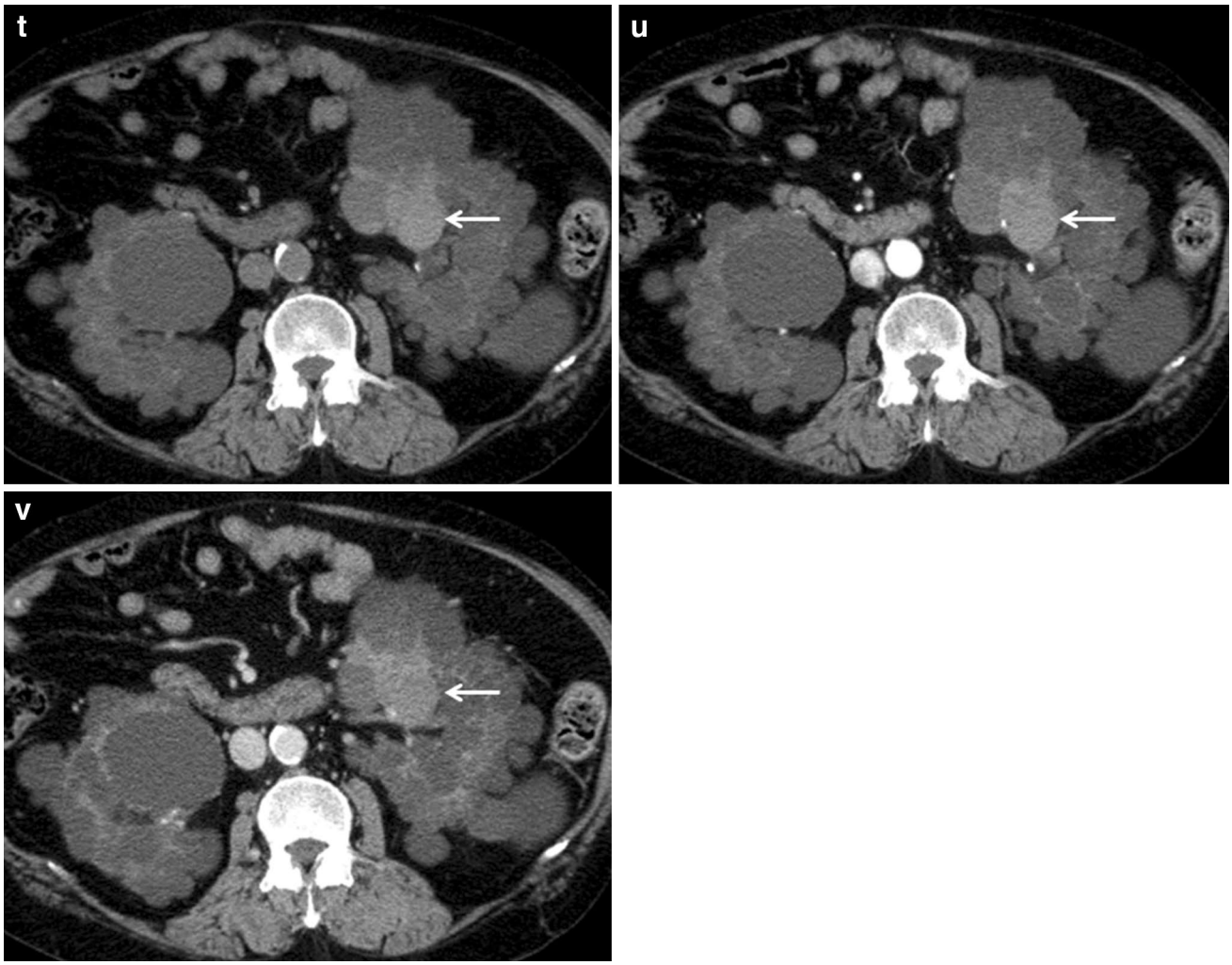

Fig. 1 (continued)

contrast-enhanced CT in our series. FDG-PET/CT may have limitations for detecting clear cell RCC, while dynamic contrast-enhanced CT may be insufficient for detection of ACD-associated RCC. Our results suggest that ^{11}C-choline PET/CT is useful for detection of RCC in patients with ACDK. Nevertheless, further investigations with larger series of patients are required to validate these initial observations.

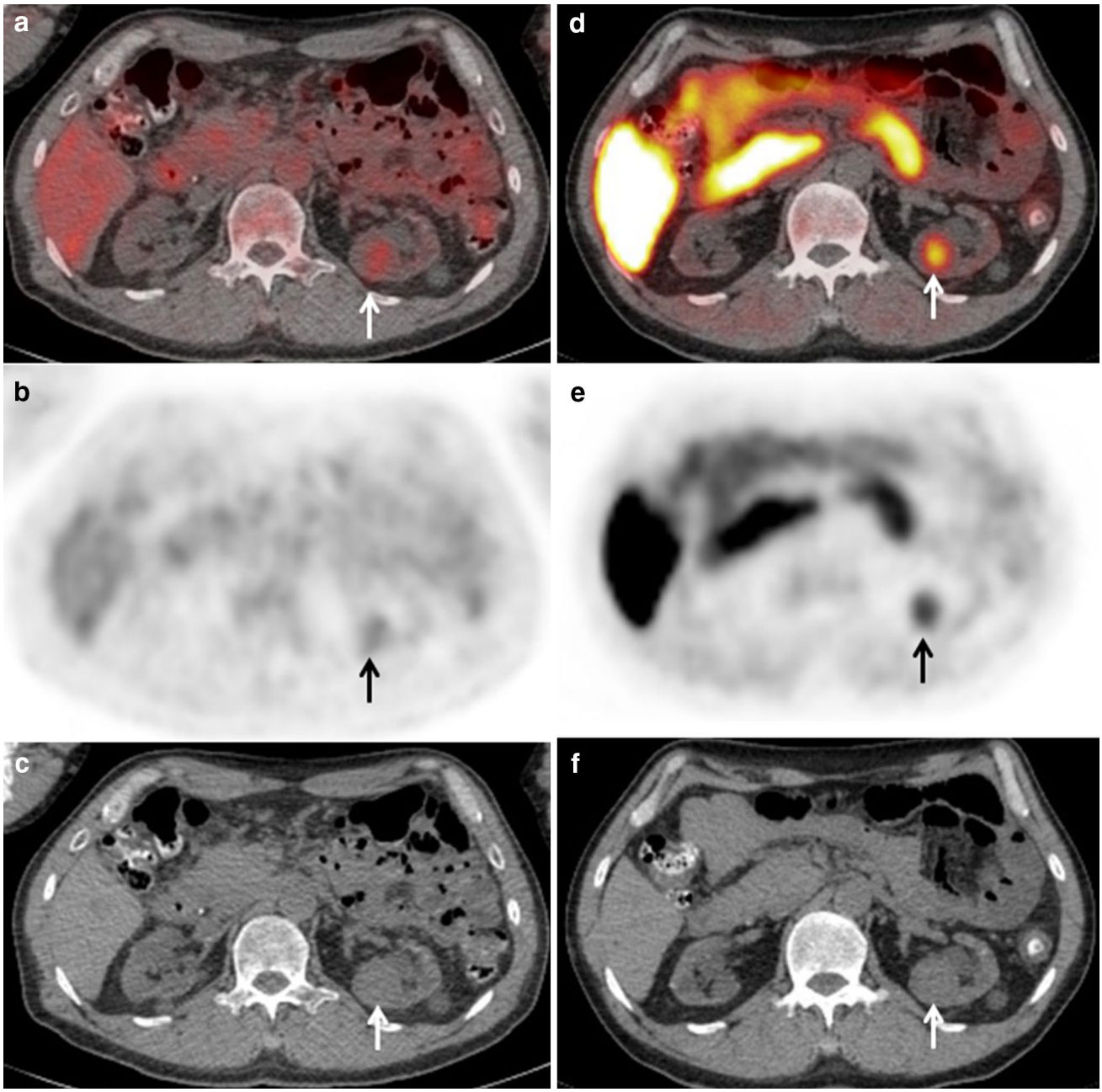

Fig. 2 Left side acquired cystic disease-associated renal cell carcinoma (ACD-associated RCC) in a 48-year-old male with acquired cystic disease of the kidney. Axial **a** FDG-PET, **b** CT, and **c** fused FDG-PET/CT showing faint FDG uptake (SUVmax 2.86) in left renal mass (arrows). Axial **d** ^{11}C-choline PET, **e** CT, and **f** fused ^{11}C-choline PET/CT showing moderate ^{11}C-choline uptake (SUVmax 3.73) in left renal mass (arrows). **g–i** Dynamic contrast-enhanced CT showing a hypervascular 2.6-cm sized left renal mass (arrows) corresponding to the same lesion shown in **a–f**. The tumor attenuation values in the **g** pre-contrast, **h** corticomedullary, and **i** nephrographic phases were 16, 20, and 32 HU, respectively

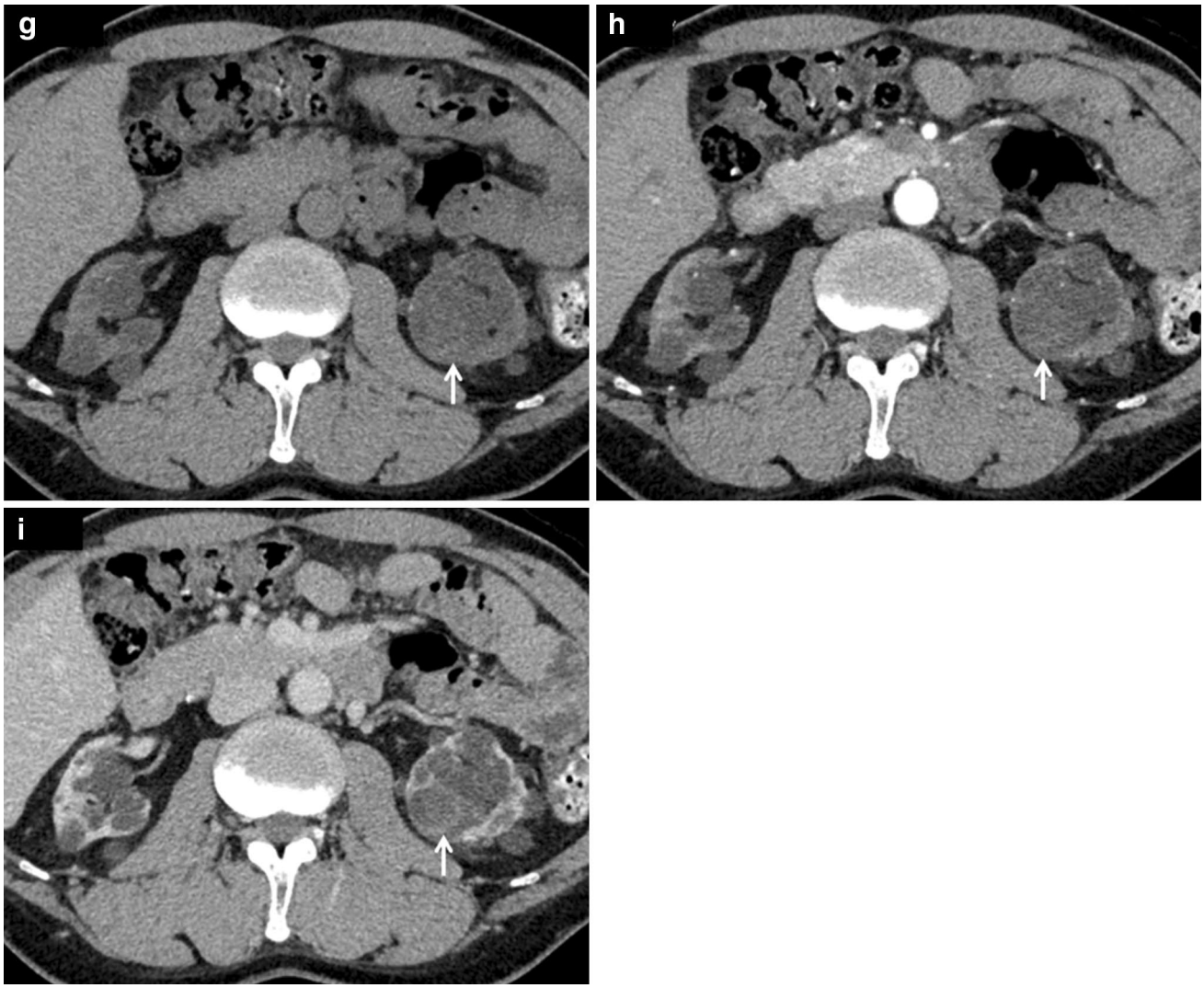

Fig. 2 (continued)

Compliance with ethical standards

Ethical approval We clearly state that human participants have the approval of an appropriate named ethics committee including Helsinki declaration.

Conflict of interest We declare no financial support or relationship that may pose conflict of interest. The authors confirm that this manuscript has not been published or presented elsewhere, in part or in entirety, and is not under consideration by any other journal. All authors have made substantial contributions to this work and have read and approved the final submitted version.

References

1. Ishikawa I. Uremic acquired renal cystic disease. Natural history and complications. Nephron. 1991;58:257–67.
2. Farivar-Mohseni H, Perlmutter AE, Wilson S, Shingleton WB, Bigler SA, Fowler JE Jr. Renal cell carcinoma and end stage renal disease. J Urol. 2006;175:2018–20 **(discussion 2021)**.
3. Tickoo SK, dePeralta-Venturina MN, Harik LR, Worcester HD, Salama ME, Young AN, et al. Spectrum of epithelial neoplasms in end-stage renal disease: an experience from 66 tumor-bearing kidneys with emphasis on histologic patterns distinct from those in sporadic adult renal neoplasia. Am J Surg Pathol. 2006;30:141–53.
4. Foshat M, Eyzaguirre E. Acquired cystic disease-associated renal cell carcinoma: review of pathogenesis, morphology,

ancillary tests, and clinical features. Arch Pathol Lab Med. 2017;141:600–6.
5. Heinz-Peer G, Maier A, Eibenberger K, Grabenwöger F, Kreuzer S, Ba-Ssalamah A, et al. Role of magnetic resonance imaging in renal transplant recipients with acquired cystic kidney disease. Urology. 1998;51:534–8.
6. Levine E. Renal cell carcinoma in uremic acquired renal cystic disease: incidence, detection, and management. Urol Radiol. 1992;13:203–10.
7. Gulanikar AC, Daily PP, Kilambi NK, Hamrick-Turner JE, Butkus DE. Prospective pretransplant ultrasound screening in 206 patients for acquired renal cysts and renal cell carcinoma. Transplantation. 1998;66:1669–72.
8. Cho C, Friedland GW, Swenson RS. Acquired renal cystic disease and renal neoplasms in hemodialysis patients. Urol Radiol. 1984;6:153–7.
9. Takebayashi S, Hidai H, Chiba T, Takagi H, Koike S, Matsubara S. Using helical CT to evaluate renal cell carcinoma in patients undergoing hemodialysis: value of early enhanced images. AJR Am J Roentgenol. 1999;172:429–33.
10. Ferda J, Hora M, Hes O, Reischig T, Kreuzberg B, Mírka H, et al. Computed tomography of renal cell carcinoma in patients with terminal renal impairment. Eur J Radiol. 2007;63:295–301.
11. Rofsky NM, Weinreb JC, Bosniak MA, Libes RB, Birnbaum BA. Renal lesion characterization with gadolinium-enhanced MR imaging: efficacy and safety in patients with renal insufficiency. Radiology. 1991;180:85–9.
12. Akita H, Jinzaki M, Akita A, Mikami S, Oya M, Kuribayashi S. Renal cell carcinoma in patients with acquired cystic disease of the kidney: assessment using a combination of T2-weighted, diffusion-weighted, and chemical-shift MRI without the use of contrast material. J Magn Reson Imaging. 2014;39:924–30.
13. Ishikawa I, Morita K, Hayama S, Nakazawa T, Araki I, Higashi K, et al. Imaging of acquired cystic disease-associated renal cell carcinoma by contrast-enhanced ultrasonography with perflubutane microbubbles and positron emission tomography-computed tomography. Clin Exp Nephrol. 2011;15:136–40.
14. Nakanishi Y, Kitajima K, Yamada Y, Hashimoto T, Suzuki T, Go S, et al. Diagnostic performance of ^{11}C-choline PET/CT and FDG PET/CT for staging and restaging of renal cell cancer. Ann Nucl Med. 2018. https://doi.org/10.1007/s12149-018-1287-3 **(Epub ahead of print)**.
15. Hara T, Yuasa M. Automated synthesis of [^{11}C]choline, a positron-emitting tracer for tumor imaging. Appl Radiat Isot. 1999;50:531–3.
16. Curry NS. Small renal masses (lesions smaller than 3 cm): imaging evaluation and management. AJR Am J Roentgenol. 1995;164:355–62.
17. Kuo PH, Kanal E, Abu-Alfa AK, Cowper SE. Gadolinium-based MR contrast agents and nephrogenic systemic fibrosis. Radiology. 2007;242:647–9.
18. Kitajima K, Yamamoto S, Fukushima K, Minamimoto R, Kamai T, Jadvar H. Update on advances in molecular PET in urological oncology. Jpn J Radiol. 2016;34:470–85.
19. Middendorp M, Maute L, Sauter B, Vogl TJ, Grünwald F. Initial experience with ^{18}F-fluoroethylcholine PET/CT in staging and monitoring therapy response of advanced renal cell carcinoma. Ann Nucl Med. 2010;24:441–6.
20. Kitajima K, Fukushima K, Yamamoto S, Kato T, Odawara S, Takaki H, et al. ^{11}C-Choline positive but ^{18}F-FDG negative pancreatic metastasis from renal cell carcinoma on PET. Nagoya J Med Sci. 2017;79:273–7.

Affiliations

Kazuhiro Kitajima[1] · Shingo Yamamoto[2] · Yusuke Kawanaka[3] · Takayuki Katsuura[1] · Masahiro Fujita[1] · Yukako Nakanishi[2] · Yusuke Yamada[2] · Takahiko Hashimoto[2] · Toru Suzuki[2] · Shuken Go[2] · Akihiro Kanematsu[2] · Michio Nojima[2] · Koichiro Yamakado[3]

Shingo Yamamoto
shingoy@hyo-med.ac.jp

Yusuke Kawanaka
n_you_634@yahoo.co.jp

Takayuki Katsuura
t-katsu@hyo-med.ac.jp

Masahiro Fujita
ma-fuzita@hyo-med.ac.jp

Yukako Nakanishi
yukakon@hyo-med.ac.jp

Yusuke Yamada
yamada80@hyo-med.ac.jp

Takahiko Hashimoto
th-uro@hyo-med.ac.jp

Toru Suzuki
tosuzuki@hyo-med.ac.jp

Shuken Go
wuxian@hyo-med.ac.jp

Akihiro Kanematsu
aqui@hyo-med.ac.jp

Michio Nojima
nojimam@hyo-med.ac.jp

Koichiro Yamakado
ko-yamakado@hyo-med.ac.jp

[1] Division of Nuclear Medicine, Department of Radiology, PET Center, Hyogo College of Medicine, 1-1 Mukogawa-cho, Nishinomiya, Hyogo 663-8501, Japan

[2] Department of Urology, Kidney Transplant Center, Hyogo College of Medicine, 1-1 Mukogawa-cho, Nishinomiya, Hyogo 663-8501, Japan

[3] Department of Radiology, Hyogo College of Medicine, 1-1 Mukogawa-cho, Nishinomiya, Hyogo 663-8501, Japan